Gaussian beam shaping based on multimode interference

X. Zhu, A. Schülzgen, H. Li, J. V. Moloney, and N. Peyghambarian

College of Optical Sciences, the University of Arizona, 1641 East University Boulvard, Tucson, Arizona 85721, USA

ABSTRACT

Laser beam transformation utilizing the effect of multimode interference in multimode (MM) optical fiber is thoroughly investigated. When a Gaussian beam is launched to an MM fiber, multiple eigenmodes of the MM fiber are excited. Due to interference of the excited modes, optical fields that vary with the MM fiber length and the signal wavelength are generated at the output facet of the MM fiber. Diffractive propagation of these confined fields can yield various desired intensity profiles in free space. Our calculations show that, an input fundamental Gaussian beam can be transformed to frequently desired beams including top-hat, donut-shaped, taper-shaped, and low-divergence Bessel-like within either the Fresnel or the Fraunhofer diffraction range, or even in both ranges. Experiments on a monothic fiber beam transformers consisting of a short piece of MM fiber (~ 10 mm long) and a single-mode signal delivery fiber were carried out. The experimental results indicate the functionality and high versatility of this simple fiber device. The performance of this fiber device can be easily and widely manipulated through parameters including the ratio between the core diameters of the SM and MM fiber segments and the length of the MM fiber segment. In addition, the intensity profile of the output beam can be controlled by tuning the signal wavelength even after the fiber device is fabricated. Most importantly, this technique is highly compatible with the technology of high power fiber lasers and amplifiers and fiber delivery systems.

Key Words: Beam shaping, multimode interference, diffraction, fiber device.

I. INSTRUCTION

Laser beams with intensity profiles other than Gaussian or with specific multimode distributions have attracted much interest with applications in laser processing, lithography, fiber injection, medical applications, and laboratory research. Laser beam shaping that redistributes the irradiance and phase of an incident beam (usually Gaussian beam) to achieve a desired intensity distribution has been intensively studied using techniques of segmentation, apodization, multifaceted integrators, and field mapping [1, 2]. Refractive, diffractive, and reflective optical components are usually used in existing beam shaping systems. However, all these optical components need careful alignment and are not compatible with optical fibers, which are extensively utilized to deliver high intense laser radiation to the work place with great operational flexibility and minimal energy loss.

In order to overcome the disadvantage of bulk elements and offer compatibility with fiber delivery systems, different fiber-based beam shapers have been proposed. Most common fiber-based beam shaping techniques use highly multimode (MM) fibers to homogenize the field distribution and generate a flat-top beam profile with circular or square

Laser Resonators and Beam Control XII, edited by Alexis V. Kudryashov, Alan H. Paxton, Vladimir S. Ilchenko, Lutz Aschke,
Proc. of SPIE Vol. 7579, 75790M · © 2010 SPIE · CCC code: 0277-786X/10/$18 · doi: 10.1117/12.840981

shape [3-5]. However, special MM fibers (hollow-core, silver-halide, and air-clad square core fibers) have to be developed for these methods and such MM fiber segments must be long enough to achieve the desired flat-top intensity distribution. Moreover, these MM fibers are not compatible with single-mode fibers that are usually used for Gaussian laser beam delivery.

Very recently, all-fiber single-mode (SM) Gaussian beam shaping devices are attracting more and more interest since they are not only compact, monolithic, and alignment-free, but also compatible with fiber lasers and fiber delivery systems that have been extensively used in different fields. Most importantly, the beam transformation is accomplished in a coherent approach. Several techniques have been reported in the literature. Top-hat beam profiles have been formed in the Fresnel diffraction region by all-fiber based beam shapers in which a long-period fiber Bragg grating (FBG) [6] and an abrupt SM fiber taper [7] were used. However, the first method requires special equipments to fabricate the grating and is limited to discrete wavelengths and the manufacturing process of fiber tapers used in the second method is hard to control and lacks reproducibility. In [8], a simple all-fiber beam shaper consisting of a short piece of large-core MM fiber and an SM signal delivery fiber was proposed. However, only ring-shaped intensity profiles have been generated within a distance of less than 100 μm away from the MM fiber facet. In fact, substantial experiments on similar fiber devices show that nondiffracting beam is more likely to be generated in the Fresnel range when large-core MM fibers were used [9]. In this paper, we report a thorough investigation of beam shaping using the same fiber structure as in [8] and [9]. It is found that, various beam intensity profiles including top-hat, donut-shaped, taper-shaped, and Bessel-like can be generated in free space at a large range of distances from the fiber facet, i.e. in the Fresnel or the Fraunhofer diffraction range, or even in both ranges.

II. THOERY AND SIMULATION

The design of the fiber device is schematically shown in Fig. 1. A short-piece of MM fiber (10 mm long or shorter) is directly spliced onto an SM signal delivery fiber. Since the performance of this fiber device can be manipulated through the wavelength of the launched light [9], a wavelength tunable laser source with narrow linewidth is generally used as the signal source.

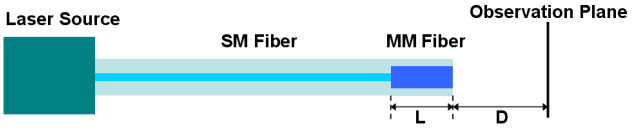

Fig. 1. Design of an all-fiber device for laser beam shaping (the figure is not to scale).

The operation principle of the fiber device shown in Fig. 1 can be described as follows: in the plane of the splicing point (z = 0), the fundamental $LP_{0,1}$ mode [$E_{SM}(r, \phi)$] of the SM fiber is coupled to the MM fiber where $LP_{0,n}$ modes [$e_n(r, \phi)$, n is the radial index] are excited exclusively due to symmetric on-axis excitation and mode orthogonality, i.e.,

$$E_{SM}(r,\phi,z=0) = \sum_{1}^{N} C_n e_n(r,\phi,z=0) \quad , \tag{1}$$

Where N is the number of excited modes inside the MM fiber, C_n is the mode expansion coefficient and can be determined from

$$C_n = \frac{\iint_S E_{SM}(r,\phi) \times e_n^*(r,\phi) ds}{\iint_S |e_n(r,\phi)|^2 ds} . \quad (2)$$

Neglecting mode conversion that may be caused by external press and structure imperfects, all excited modes propagate independently inside the MM fiber, and the field $E_{MM}(r, \phi, z)$ along the MM fiber can be expressed as

$$E_{MM}(r,\phi,z) = \sum_1^N C_n e_n(r,\phi,0) e^{-i\beta_n z} , \quad (3)$$

where β_ns are the propagation constants of the n-th excited mode of the MM fiber. Due to the interference of the multiple modes, the field $E_{MM}(r, \phi, z)$ has various distributions at different positions as shown in Fig. 2, where the input field is the fundamental mode of a conventional SM fiber (SMF-28) and the MM fiber has a diameter of 50 μm. At some specific positions such as 8 mm and 10.36 mm shown in Fig. 2, the input field $E_{SM}(r, \phi)$ is reproduced and the phenomenon is called self-imaging. The self-imaging effect in MM fibers was first observed by Allison [10] and has been experimentally demonstrated by several groups in recent years for various applications such as wavelength tunable laser [11], all-fiber bandpass filter [12], wavelength tunable fiber lens [13], fiber-optic displacement sensor [14], and MMI-based fiber lasers [15-17]. For the application of beam shaping, the field at other positions will be of much interest, so the MM fiber is generally cleaved with a certain length L not equal to the self imaging length. The field at the output facet of the MM fiber can then be written as

$$E_{Out}(r,\phi,L) = \sum_{n=1}^N C_n e_n(r,\phi) e^{-i\beta_n L} , \quad (4)$$

Diffractive propagation of the field described by Eq. (4) produces various intensity profiles in free space. Thus, the input Gaussian beam is transformed to a beam with various profiles at different positions.

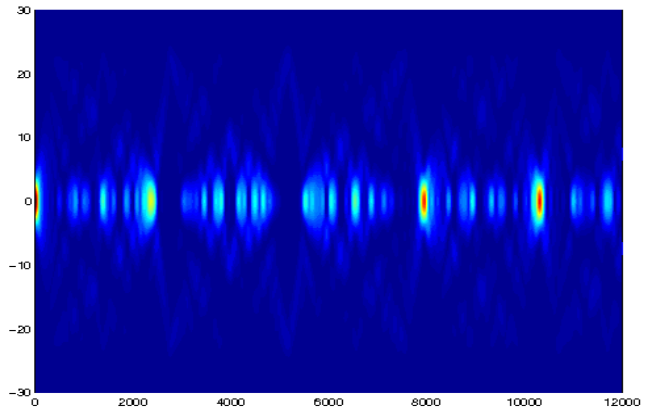

Fig. 2. The lateral distribution of the field $E_{MM}(r, \phi, z)$ along the propagation direction in the 50 μm MM fiber.

To investigate the characteristics of this fiber-based beam shaper, the free space propagation of the beam exiting the monolithic fiber device that consists of a conventional SM fiber (SMF-28) and an MM fiber with a diameter of 50 μm is calculated. The fully vectorial mode expansion approach, developed by Li [18], is used to do the calculation of C_ns in Eq. (4) and determine the facet field E_{out}. The field distributions in observation planes between 1 mm and 20 mm away from the fiber facet are obtained using Fresnel diffraction in cylindrical coordinates:

$$E_{fs}(r,\phi) = \frac{1}{i\lambda D} e^{i\frac{\pi r^2}{\lambda D}} \iint_{S'} E_{out}(r',\phi') e^{i\frac{\pi r'^2}{\lambda D}} J_0\left(\frac{2\pi r' r}{\lambda D}\right) ds', \tag{5}$$

where r' and ϕ' are the coordinates at the fiber facet, and D is the distance from the observation plane to the fiber facet. The field distributions in the near-field planes with a distance less than 1 mm have been calculated using the transfer function in free space [19]:

$$E_{fs}(r,\phi) = FT^{-1}\left\{FT\left[E_{out}(r',\phi')\right]\exp\left[i\frac{2\pi D}{\lambda}\sqrt{1-(\lambda\xi)^2-(\lambda\eta)^2}\right]\right\}, \tag{6}$$

where ξ and η are spatial frequencies of the facet field and FT and FT^{-1} represent a 2-dimensional Fourier transformation and an inverse Fourier transformation, respectively.

According to equation (4), the field distribution at the facet of the MM fiber depends on the MM fiber length (L) and the propagation constant, which is wavelength (λ) dependent. Thus, a large variety of fields confined to the MM fiber core can be created at the fiber facet by controlling the variables L and λ. For instance, when the fiber length is 9.5 mm and the signal wavelength is 1535 nm, the facet field is shown in Fig. 3 (a). The lateral distribution of the beam propagating in the 1200 μm free space region is plotted in Fig. 3(b). When the fiber length increases to 10 mm, the facet field as shown in Fig. 4(a) is much different from that of 9.5 mm [Fig. 3(a)]. Consequently, the beam profile also exhibits a significantly different feature shown in Fig. 4(b). Therefore, various facet fields can be generated by controlling the MM fiber length and consequently different beam profiles can be obtained in free space as analyzed above. When the signal wavelength is 1572 nm and the fiber length is 10 mm, the facet field is plotted in Fig. 5(a) and the lateral distribution of the near field is shown in Fig. 5(b). As the signal wavelength changes to 1580 nm, the facet field and the lateral intensity distribution are plotted in Fig. 6(a) and (b), respectively. Evidently, the performance of this fiber device also depends on the signal wavelength.

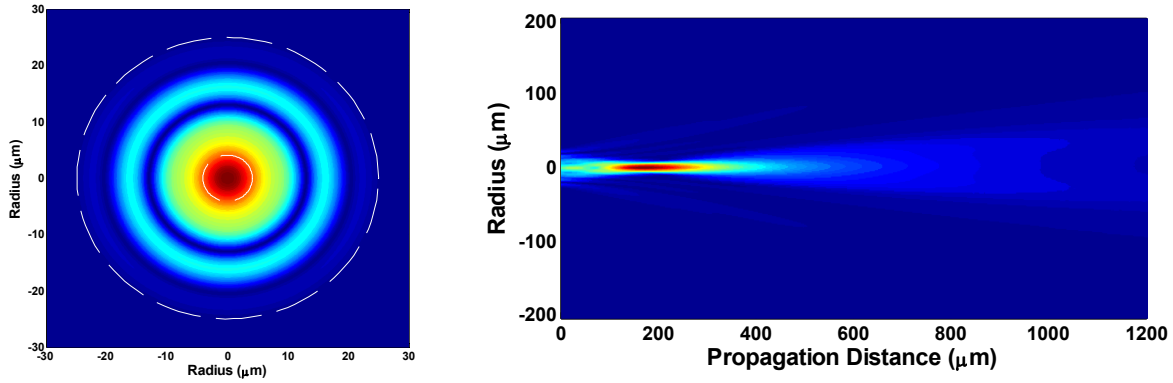

Fig. 3. (a) Distribution of the facet field of a 9.5 mm long 50 μm multimode fiber and (b) the corresponding near-field lateral intensity profiles when the signal wavelength is 1535 nm.

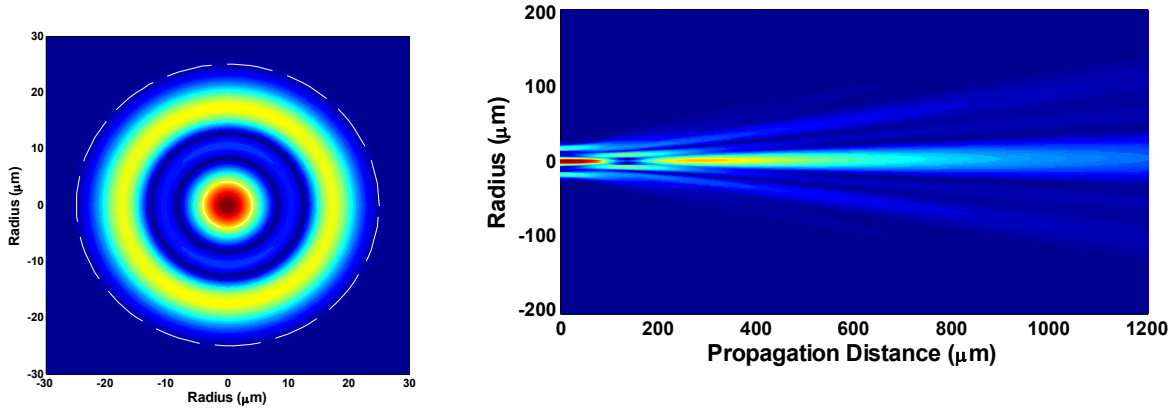

Fig. 4. (a) Distribution of the facet field of a 10 mm long 50 μm multimode fiber and (b) the corresponding near-field lateral intensity profiles when the signal wavelength is 1535 nm.

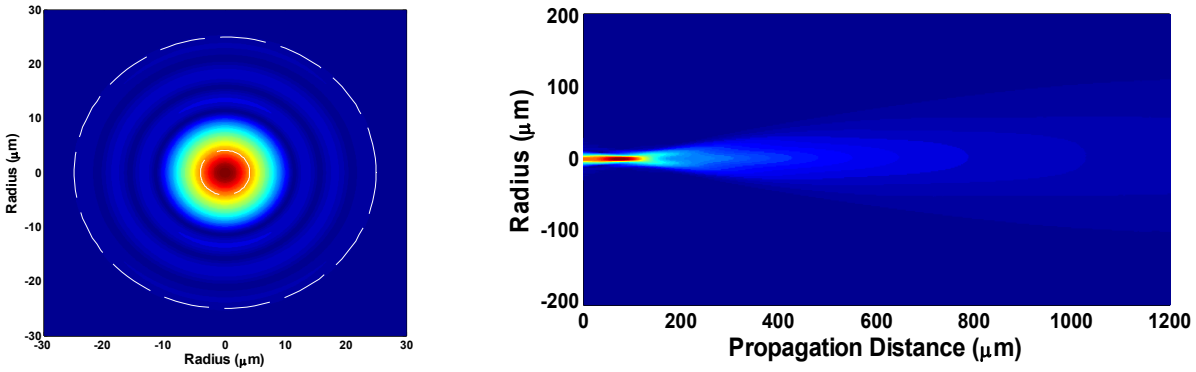

Fig. 5. (a) Distribution of the facet field of a 10 mm long 50 μm multimode fiber and (b) the corresponding near-field lateral intensity profiles when the signal wavelength is 1572 nm.

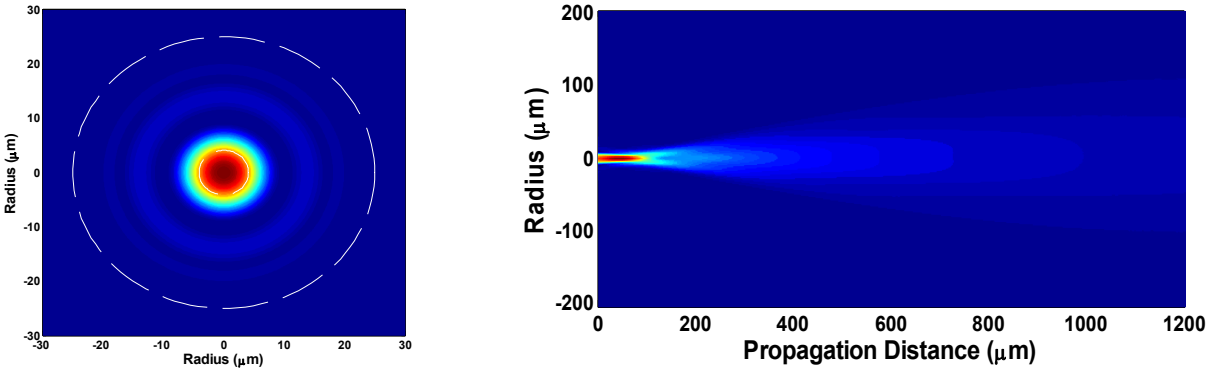

Fig. 6. (a) Distribution of the facet field of a 10 mm long 50 μm multimode fiber and (b) the corresponding near-field lateral intensity profiles when the signal wavelength is 1580 nm.

For the case shown in Fig. 5, the intensity distribution of the beam exiting the MM fiber at selected planes in free space is plotted in Fig. 7. Clearly, a top-hat beam is generated in both the Fresnel and the Fraunhofer diffraction regions starting from 800 μm. In contrast, for the case shown in Fig. 6, a top-hat beam can be generated only in Fresnel region of 500-1000 μm near the fiber facet as shown in Fig. 8. Therefore, the plane where a desired beam profile is created can be varied by slightly changing the signal wavelength. In addition, according to the properties of MMI in MM waveguides [9, 15, 16], the location of a desired beam profile can also be varied by changing the length of the MM fiber. In other words, a desired intensity profile in the far-field region can be shifted to the near-field region by changing the signal wavelength or the length of the MM fiber. Thus, far-field intensity profiles are mainly considered in this paper.

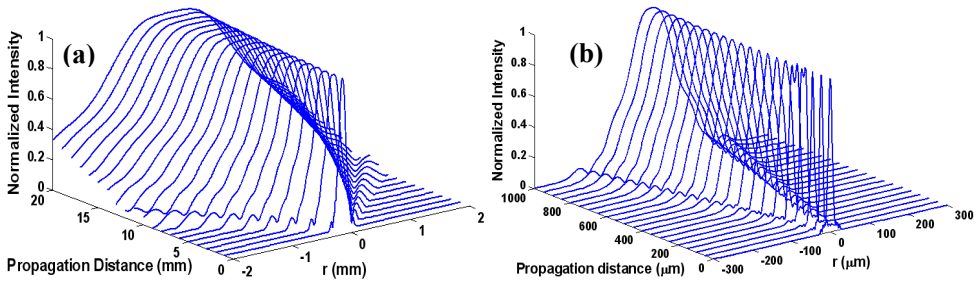

Fig. 7. Intensity distribution of the laser beam propagating in free space when the signal wavelength is 1572 nm. (a) The plot ranges from 1 mm to 20 mm; (b) the plot ranges from 0 mm to 1 mm.

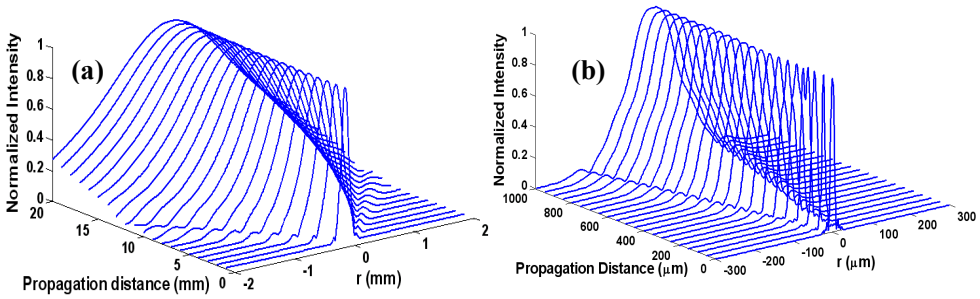

Fig. 8. Intensity distribution of the laser beam propagating in free space when the signal wavelength is 1580 nm. (a) The plot ranges from 1 mm to 20 mm; (b) the plot ranges from 0 mm to 1 mm.

According to Fraunhofer diffraction theory, a desired intensity profile can be obtained in the far-field if a field corresponding to its inverse Fourier transformation is generated at the output facet of the MM waveguide. Because the facet field $E_{out}(r,\phi,z)$ is easily changeable, most desired beam profiles can be generated in the far-field by properly tailoring the MM fiber and changing the signal wavelength. For the case of beam transformation shown in Figs. 5 and 7, where the signal wavelength is 1572 nm and the MM fiber length is 10 mm, the intensity profile of the top-hat beam at a distance of 20 mm from the MM fiber facet is redrawn by the red line in Fig. 9. As the signal wavelength changes to 1525 nm, a donut-shaped beam is created and its intensity distribution is plotted as blue curves in Fig. 9. When the signal wavelength changes to 1559 nm, a taper-shaped far-field is created. The intensity profile is plotted as green curves. When the length of the MM fiber segment is changed from 10 mm to 11 mm the performance of the fiber device is different. A Bessel-like beam with a low-divergence central spot is always generated. For a signal wavelength of 1555 nm the intensity profile of the Bessel-like beam at a distance of 20 mm and its corresponding facet field are plotted by black curves in Fig. 9 (a) and (b), respectively.

Based on the calculation results of the 50 μm MM fiber above, it is reasonable to draw a conclusion that beam transformation based on MMI exhibits a versatile functionality and most desired beams can be obtained at any plane in free space by changing the parameters that determine the facet field, i.e. the signal wavelength and the length of the MM fiber segment,.

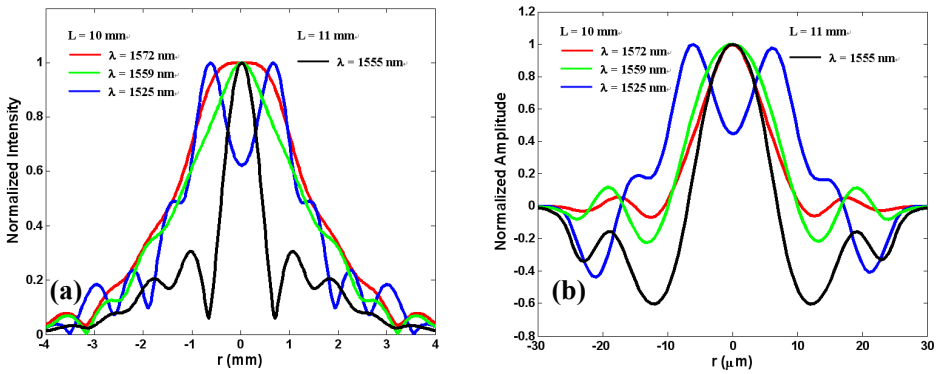

Fig. 9. (a) Four often desired intensity profiles generated at a distance of 20 mm from the fiber facet and (b) the corresponding field distribution at the MM fiber facet. Red curve (top-hat); green curve (taper-shaped); red curve (donut-shaped); black curve (Bessel-like).

III. EXPERIMENTS

Experimental investigations of beam transformation based on MMI were accomplished with the monolithic fiber device that is schematically shown in Fig. 1. The signal delivery fiber is conventional SM fiber (SMF-28) with a core diameter of 8.2 μm and a NA of 0.14. The beam shaping fiber has a diameter of 50 μm and a NA of 0.22. A single-frequency semiconductor laser (Agilent, Model 81680A) with a wavelength tuning range from 1456 nm to 1584 nm was applied as the signal source. An infrared CCD camera (Electrophysics, Model 7290 A) was used to record the intensity profiles in observation planes.

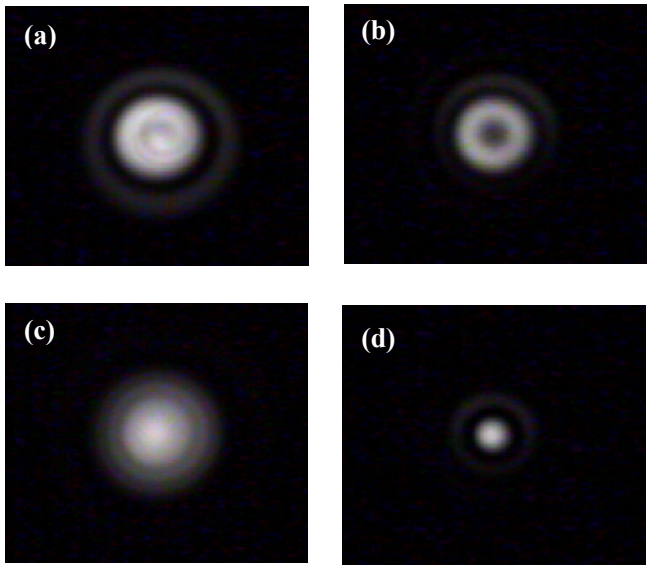

Fig. 10. (a) top-hat, (b) donut-shaped, (c) taper-shaped, and (d) Bessel-like intensity profiles created experimentally and recorded by a CCD camera at a distance of 20 mm from the MM fiber facet.

Experiments were carried out with several pieces with lengths around 10 mm in approximation of the idealized simulation studies. The generated intensity patterns were recorded by the CCD camera at a 20 mm distance from the MM fiber facet and prominent examples are shown in Fig. 10. The normalized distributions of the intensity profiles are plotted in Fig.11. For comparison, the far-field intensity profile of light exiting directly from the SM fiber is included. When the MM fiber length is 10 mm and the signal wavelength is between 1556 nm and 1568 nm, a top-hat beam can be created. At a wavelength of 1561 nm, the top-hat beam has the widest top. Its image and intensity profile are shown in Fig. 10(a) and Fig. 11(a), respectively. The uniformity of the top-hat beam in the central 1.8 mm is within a few percent when it is measured by a scanning slit of 2 μm width. In contrast, a donut-shaped beam is obtained as the signal wavelength changes to 1515-1523 nm and 1478-1496 nm. When the signal wavelength is 1482 nm, a donut-shaped beam with the lowest central intensity is obtained and is shown in Fig. 10(b). Its intensity profile is plotted in Fig. 11(b). Although a taper-shaped beam is created when the wavelength is 1550 nm and the MM fiber length is 10mm, a taper-shaped beam with a much better linear slope [shown in Fig. 10(c) and Fig. 11(c)] is obtained when the MM fiber

length is 10.1 mm and the signal wavelength is 1567 nm. Finally, a low-divergence Bessel-like beam with the highest central intensity is obtained [shown in Fig. 10(d)] when the MM fiber length is 10.9 mm and the signal wavelength is 1534 nm. In this case, the divergence angle of the central spot is less than a fourth of that of the input Gaussian beam as shown in Fig. 11(d). Clearly, the experimental results indicate the functionality and high versatility of this simple fiber device. Slightly deviating features in the intensity distributions can be attributed to imperfect connections between SM fiber and MM fiber segments as well as interference effects occurring at the detector plane of the CCD camera.

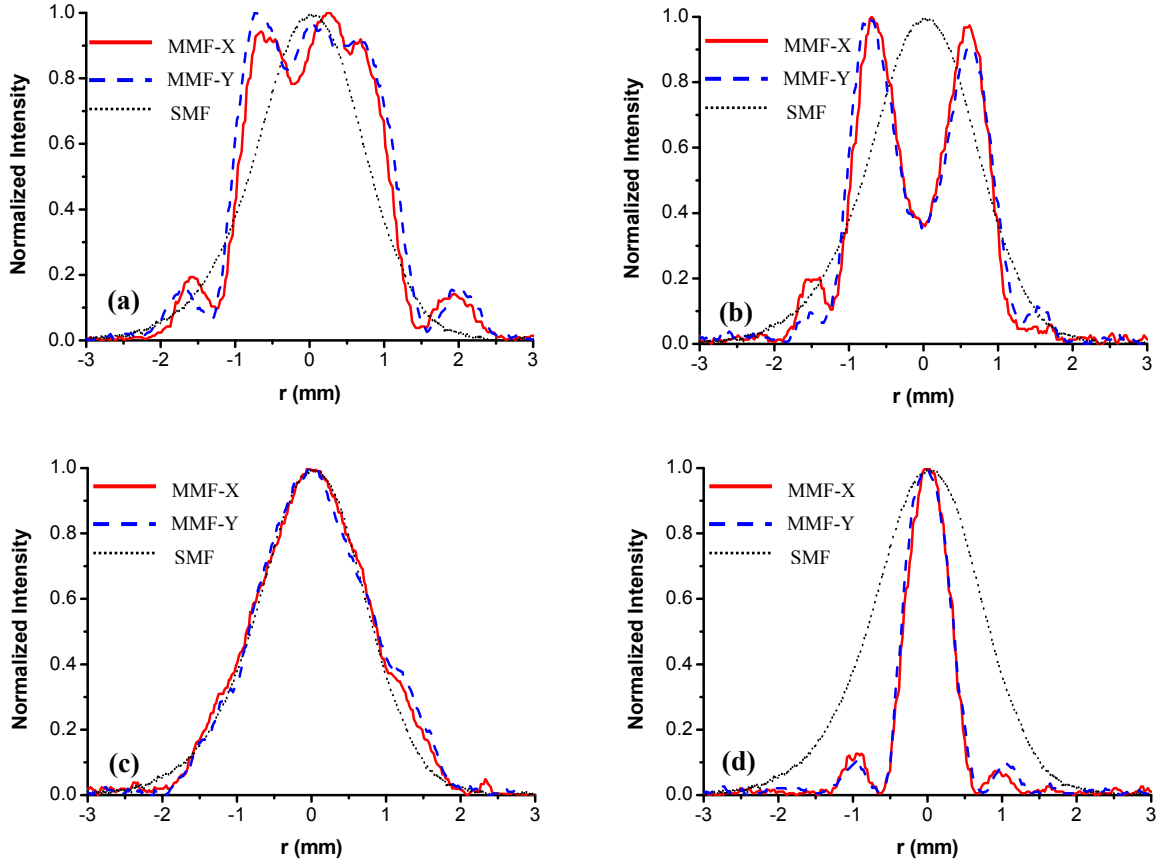

Fig. 11. Normalized radial distributions of (a) top-hat, (b) donut-shaped, (c) taper-shaped, and (d) Bessel-like intensity profiles created experimentally at a distance of 20 mm from the MM fiber facet.

Not that, this all-fiber based technique is highly compatible with the technology of high power fiber lasers and amplifiers and fiber delivery systems. With the advances of high power fiber lasers and amplifiers, large-mode-area (LMA) SM fibers are usually used to suppress nonlinear effects and scale up the handling power. Desired beam profiles can be obtained by using an MM fiber with a larger core diameter as the mode field diameter of the signal delivery fiber becomes larger.

IV. DISCUSSION AND CONCLUSION

Beam shaping based on MMI is a coherent beam transformation. Diffraction of the confined facet field can generate desired beams in free space. Our calculations show that, in addition to generating a top-hat beam like a beam homogenizer does, a short piece of MM fiber can transform an input Gaussian beam to a donut-shaped, a taper-shaped, or a Bessel-like beam. Comparing to beam homogenizers, beam transformers based on MMI exhibit superior functionality and high versatility.

Analysis and characterization of a simple and compact all-fiber beam transformer show that an input Gaussian beam can be transformed to various desired beams. The performance of this fiber device can be easily and widely manipulated by changing the length of the MM fiber segment. Due to the dispersion of the propagation constants, the intensity profile of an output beam as well as its location can be controlled by tuning the signal wavelength. It is worth mentioning that, the desired intensity profiles can be generated in the Fresnel or the Fraunhofer diffraction range, or even in both ranges. In particular, collimated desired beam profiles can be obtained by using a fiber collimator if they are formed in the far-field region.

Beam transformation techniques based on MMI in MM fibers enable compact, monolithic, and alignment-free all-fiber beam shaping devices with high flexibility and minimal loss that are highly compatible with high power fiber lasers and amplifiers systems and fiber delivery systems. Our experimental results using commercial MM fibers agree well with the calculations. Desired beams with much better distributions that are required for some specific applications can be achieved if the MM fiber segments are precisely designed or modulated by inscribing long-period FBGs in the cores.

V. ACKNOWLEDGEMENT

This work is supported by the National Sciences Foundation through grant No. 0725479 and the state of Arizona TRIF Photonics Initiative. We would thank Hua Wei for her technical support in the simulation.

REFERENCE

1. Dickey, F. and Holswade, S., Eds., *Laser Beam Shaping: Theory and Techniques* (New York: Marcel Dekker, 2000).
2. Dickey, F., Shealy, D. and Holswade, S., Eds, *Laser Beam Shaping Applications* (New York: Marcel Dekker, 2005).
3. Matsuura, Y., Miyagi, M., German, A., Nagli, L. and Katzir, A., "Silver-halide fiber tip as a beam homogenizer for infrared hollow waveguides," Opt. Lett. **22**, 1308-1310 (1997).
4. Matsuura, Y., Akiyama, D. and Miyagi, M., "Beam homogenizer for hollow-fiber delivery system of excimer laser light," Appl. Opt. **42**, 3505--3508 (2003).
5. Hayes, J., Flanagan, J., Monro, T., Richardson, D., Grunewald, P. and Allott, R., "Square core jacket air-clad fiber," Opt. Express **14**, 10345-10350 (2006).

6. Gu, X., Mohammed, W., Qian, L. and Smith, W., "All-fiber laser beam shaping using a long-period grating," IEEE Photon. Technol. Lett. **20**, 1130-1132 (2008).
7. Tian, Z., Nix, M. and Yam, S., "Laser beam shaping using a single-mode fiber abrupt taper," Opt. Lett. **34**, 229-231 (2009).
8. Yilmaz, Y., Mehta, A., Mohammed, W. and Johnson, E., "Fiber-optic beam shaper based on multimode interference," Opt. Lett. **32**, 3170-3172 (2007).
9. Zhu, X., Schülzgen, A., Li, L. and Peyghambarian, N., "Generation of controllable nondiffracting beams using multimode optical fibers," Appl. Phys. Lett., **94**, 201102 (2009).
10. Allison S.and Gillies, G., "Observations of and applications for self-imaging in optical fibers," Appl. Opt. **33**, 1802-1805 (1994).
11. Selvas, R., Torres-Gomez, I., Martinez-Rios, A., Alvarez-Chavez, J., May-Arrioja, J., Likamwa, P., Mehta, A. and Johnson, E., "Wavelength tuning of fiber lasers using multimode interference effects," Opt. Express **13**, 9439-9445, (2005).
12. Mohammed, W., Smith, P. and X. Gu, X., "All-fiber multimode interference bandpass filter," Opt. Lett. **31**, 2547-2549, (2006).
13. Mohammed, W., Mehta, A. and Johnson, E., "Wavelength tunable fiber lens based on multimode interference," J. Lightwave Technol. **22**, 469-477, (2004).
14. Mehta, A., Mohammed, W. and Johnson, E., "Multimode interference-based fiber-optic displacement sensor," IEEE Photon. Technol. Lett. **15**, 1129-1131, (2003).
15. Zhu, X., Schülzgen, A., Li, H., Li, L., Wang, Q., Suzuki, S., Temyanko, V., Moloney, J. and Peyghambarian, N., "Single-transverse-mode output from a fiber laser based on multimode interference," Opt. Lett. **33**, 908-910 (2008).
16. Zhu, X., Schülzgen, A., Li, H., Li, L., Han, L., Moloney, J. and Peyghambarian, N., "Detailed investigation of self-imaging in large-core multimode optical fibers for application in fiber lasers and amplifiers," Opt. Express **16**, 16632-16644 (2008).
17. Zhu, X., Schülzgen, A., Li, H., Li, L., Temyanko, V., Moloney, J. and Peyghambarian, N., "High power fiber lasers and amplifiers based on multimode interference," IEEE J. Sel. Top. Quant. Electron. **15,** 71-78 (2009).
18. Sziklas, E. and Siegman, A. "Diffraction calculations using fast Fourier transform methods," Proceeding of the IEEE **62**, 410-412 (1974).
19. Li, H., Brio, M., Li, L., Schülzgen, A., Peyghambarian, N. and Moloney, J., "Multimode interference in circular step-index fibers studies with the mode expansion approach," J. Opt. Soc. Am. B **24**, 2707-2720 (2007).